Journal of the European Ceramic Society 16 (1996) 803–811

S0955-2219(96)00003-9
0955-2219/96/$15.00+.00

Grain Size Dependent Residual Microstresses in Submicron Al_2O_3 and ZrO_2

Andreas Krell,[a] Angelika Teresiak[b] & Dietrich Schläfer[b]

[a]Fraunhofer-Institut für Keramische Technologien und Sinterwerkstoffe (IKTS), D-01277 Dresden, Germany
[b]Institut für Festkörper- und Werkstofforschung Dresden, Postfach 270016, D-011071 Dresden, Germany

(Received 12 October 1995; revised version received 27 November 1995; accepted 5 December 1995)

Abstract

X-ray measurements of lattice spacings are used to determine residual microstresses present in sintered alumina and in tetragonal zirconia polycrystals due to thermal expansion anisotropy (TEA). In Al_2O_3 with grain sizes larger than 1 μm the microstresses are 30–100 MPa, in submicrometer samples the grain size influence becomes small and residual stresses range between 20 and 30 MPa. For the grain sizes between 0·3 and 9 μm there is no indication of a change in the high-temperature relaxation mechanism. In ZrO_2 with grain sizes of 0·5–1 μm the residual stresses are similar as observed in Al_2O_3 (20–60 MPa), they decrease further at grain sizes 0·2–0·4 μm. The results are independent of technological approaches like powder processing or sol/gel used to produce the sintered bodies.

1 Introduction

The need for residual stress measurements results from their complex influences on the mechanisms of the microstructural development during sintering, on crack propagation and energy dissipation, and on the macroscopic technical performance (e.g. strength, toughness, wear). Whereas the present work was focused on *micro*stresses, other components have to be considered as well because X-ray measurements on ground surfaces comprise contributions from different (microscopic and macroscopic) stress components. A threefold classification of residual stresses in polycrystals adopted here was given e.g. by Kloos.[1]

First kind residual stresses are macroscopic along at least one dimension (e.g. within a surface, possibly with a steep gradient along the perpendicular z-direction). A frequent origin is microplastic deformation (dislocations, twins)—important for all measurements on ground or polished ceramic surfaces.[2,3] The size of subsurface grinding damage decreases with smaller grain sizes.[4] Extended subsurface damage is present in the upper layer of grains only, and even in 40 μm coarse grained alumina it occurs only within a 20 or 2 μm thin surface region after grinding or polishing, respectively.[2] In sintered alumina with 2 μm grain size the resulting macroscopic residual compressive stresses are about −35 MPa in a depth of 25 μm, higher stresses of −150 MPa are present within a 10 μm thin surface layer,[5] and only the upper 1–3 layers of grains exhibit a stress level of −450 MPa.[6]

Second kind residual stresses develop on cooling of sintered polycrystals due to thermal contraction differences between the crystallites. In polyphase ceramics there is a thermal misfit between grains of different phases, in single-phase non-cubic polycrystals thermal expansion anisotropy (TEA) produces residual stresses due to the different thermal contraction of randomly oriented neighbouring grains. Sintered alumina was studied first by Evans.[7] In a first approximation these stresses do not depend on grain sizes, but their relaxation introduces an important grain size effect discussed below. Second kind residual stresses are of outstanding importance for the ratio of trans- and intergranular fracture, for crack branching or bridging,[8] microcracking,[7,9] stress-induced phase transformation,[10,11] and subcritical crack growth.[12] In this way, microstresses govern crack-propagation-induced energy dissipation[13,14] and affect the macroscopic toughness and strength. Their investigations contribute to an improved understanding of the technologically important correlation of grain size and macroscopic mechanical behaviour. These microstresses were the central subject of our study.

Third kind residual stresses on the scale of lattice defects within the grains influence the hardness and the tribological behaviour, but their effect on the macroscopic toughness and strength is usually small. These stresses are not a subject of the present investigation.

In sintered alumina with a random orientation of grains and at a temperature difference on cooling of $\Delta T = -1500$ K, a first approach gives an average tensile component $\sigma_c \approx 250$ MPa in the direction of the c-axis.[7] A more realistic evaluation has to consider the statistical character of the orientation relationship of neighbouring grains and needs statistical calculations as proposed by Kreher.[15] In his paper, simple analytical expressions for the average TEA microstresses in the grains were derived under the assumption that the elastic anisotropy of the single crystals can be neglected, i.e. one has to approximate the elastic stiffness tensor by isotropic constants. Kreher and Molinari demonstrated different approaches which can be used for this purpose,[16] but for a first qualitative estimation it is sufficient to use known macroscopic effective elastic constants of the polycrystalline materials (actually, no unambiguous anisotropic data are available for tetragonal zirconia doped with different amounts of Y_2O_3). Hence, with the exact statistical solutions derived by Kreher[15] an average tensile microstress along the c-axis is calculated for Al_2O_3 as $\sigma_c = 148$ MPa with a corresponding compressive stress $\sigma_a = -\sigma_c/2 = -74$ MPa in the plane perpendicular to the c-axis (Al_2O_3: $E \approx 400$ GPa, Poisson's ratio $\nu \approx 0{\cdot}23$, $\Delta\alpha = \alpha_c - \alpha_a = 0{\cdot}9 \times 10^{-6}$ K^{-1}, $\Delta T = -1500$ K). This result is considerably lower than Evans' approach. For zirconia the use of $E = 217$ GPa, $\nu = 0{\cdot}32$, $\Delta\alpha = 1{\cdot}55 \times 10^{-6}$ K^{-1}, $\Delta T = -1400$ K yields $\sigma_c = 126$ MPa. Figure 1 shows these stresses after an appropriate tensor transformation in the sample-fixed coordinate system as a function of the orientation of the considered grain. Note the very *similar* results in spite of the high thermal anisotropy in ZrO_2 (caused by its low Young's modulus).

Second kind TEA stresses are subject to high-temperature visco-elastic relaxation during a cooling interval when the grain boundary viscosity is yet low, and all measurements are expected to give results lower than indicated by Fig. 1. Two similar approaches describe visco-elastic relaxation in a form[17,18] that is equivalent with

$$<\sigma> = \sigma_0 + \int \frac{<\sigma> E}{\dot{T}\eta_{\text{eff}}} \, dT \qquad (1)$$

$$\eta_{\text{eff}} \sim G^2 / D_{\text{eff}} \qquad (2)$$

where $<\sigma>$ is the statistical average of the residual stress, σ_0 is the stress before relaxation, $\dot{T}$ is the cooling rate (<0!), η_{eff} is the effective grain boundary viscosity which is proportional with the square of the grain size G and with the inverse effective diffusion coefficient D_{eff}; E and ΔT have the meaning as introduced above. Due to the strong grain size effect in eqn (2), the relaxation term in eqn (1) reduces the residual stress $<\sigma>$ the smaller the grain size. With only grain boundary diffusion considered, an approximation gives $D_{\text{eff}} \sim 1/G$, and the grain size effect can be described by $<\sigma> = \sigma_0 - (1/G^3) \int A \, dT$ where a term with an inverse grain size appears which is not affected by the integration.[18] However, the limitations of the validity of such approximations are not obvious, and none of the models claims a simple stress–grain size relationship. On the contrary, Blendell and Coble emphasize the requirement of a numerical integration (in their work this procedure gives a rather weak grain size effect: 6 MPa difference for grain sizes between 50 and 150 MPa).

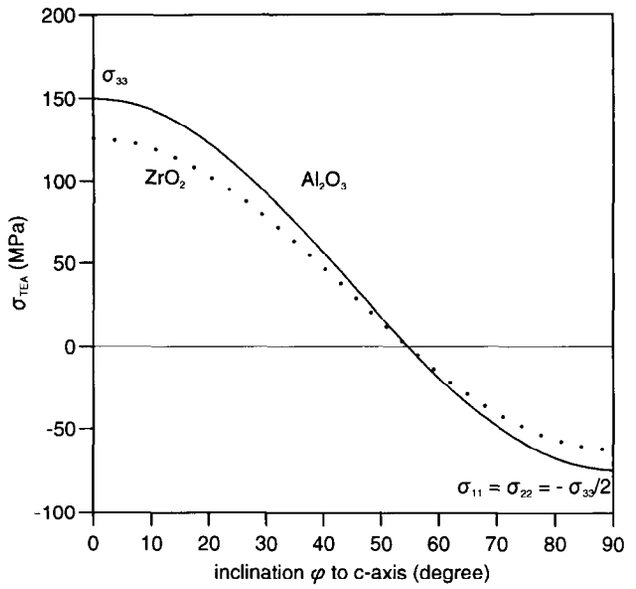

Fig. 1. Theoretical evaluation of residual stresses σ_{TEA} in Al_2O_3 and ZrO_2. The shape of the curve with the given relationship of σ_{33} and σ_{11} and with zero stresses at 55° is a consequence of the tensor transformation and the required balance of forces.

With relaxation stimulated by progressively smaller grain sizes, the driving force $<\sigma>$ of the relaxation term in eqn (1) decreases. Therefore, whereas $<\sigma>$ decreases continuously with reduced grain sizes, the *degree* of the grain size influence will decrease significantly at very small grain sizes.

Elaborated X-ray diffraction methods measure macroscopic first and second kind surface stresses when the average of the stress over the examined phase is not zero ($\sin^2 \psi$ approach; ψ is the angle between the normals of the specimen surface and of diffracting {hkl}-planes);[19,20] it is also possible to incorporate the effect of elastic anisotropy into the analysis.[21] In single phase materials, however, the $\sin^2\psi$ approach cannot be used to investigate *thermal anisotropy micro*stresses in the bulk (without influences of macroscopic surface stresses) because the associated strains are fixed at each of the randomly oriented crystallites (in their isotropic surroundings). Without any relationship of these

*micro*strains to the macroscopic surface, a variation of the macroscopic direction ψ for one reflex (hkl) would find the same lattice spacing d for all ψ—an incorrect pretence of a zero strain due to the circumstance that the reflecting crystallites exhibit a constant strain independent of different ψ. Hence, second kind microstresses in single phase materials have to be derived by other techniques. Three methods were described:

(i) Precision X-ray measurements of lattice parameters comparing the sintered body with a powder standard resulted in $\sigma_c \approx 40$–70 MPa for an alumina with 3 μm grain size; there were indications of increasing relaxation with increasing impurity and doping concentrations (MgO, SiO_2, PbO).[22] This result is in fair qualitative agreement with Fig. 1 if one assumes a high degree of relaxation.

(ii) The same agreement holds for a measurement which analysed the broadening of spectroscopic R lines (due to Cr^{3+} impurities).[17] For 50–130 μm coarse alumina with probably low relaxation activity σ_c was 100–130 MPa.

(iii) Inconsistent results were derived from a new method which analyses the frequency shift of the optical fluorescence from Cr^{3+} impurities. Measurements in Al_2O_3/ZrO_2 composites with alumina grain sizes of 2–8 μm resulted in $\sigma_c = 56$ MPa for the alumina phase which agrees well with other published data.[23] In single phase alumina, however, surprisingly high values ranging from 100–160 MPa (grain size 2 μm) to 200–300 MPa (16 μm) were reported.[24]

At present, attention has focused on microstructures with grain sizes smaller than 1 μm, but measurements of TEA microstresses were published for coarser grained ceramics only (in alumina for the 50–150 μm[17] and for the 2–20 μm range[24]). The present study was, therefore, concentrated on the grain size influence in σ_{TEA} microstresses down to about 0·2 μm. The comparison of residual stresses in alumina and in zirconia was intended to give an insight into the role of different grain boundary structures in both materials.

2 Materials and Methods

2.1 Materials and measurements

Table 1 gives a survey of the investigated materials. All but one sample were fabricated by usual powder processing, sintering in air and diamond grinding (40–50 μm grit size). An additional alumina batch was prepared from boehmite with a sol/gel technology (+ α-Al_2O_3 seeds <0·2 μm) to test whether TEA stresses depend on special technological approaches or on surface conditions. Therefore, this sample was broken down to a grit size of about 0·2 mm before X-ray investigations and measured in this fractured state (with a crystallite size of about 0·5 μm the broken grit size of 200 μm is large enough to represent real polycrystals with a level of residual microstresses as typical in this microstructure).

The monoclinic phase content was zero in most of the ground ZrO_2 surfaces. Only the coarsest of the zirconia microstructures (0·77 μm) exhibited a slight increase of the monoclinic content from zero to 3% on grinding.

The orientation dependent lattice strain was derived from very precise X-ray measurements of lattice parameters in the sintered bodies and in powder standards. For this procedure it is essential to have specimens and standards with the same state of possible solid solutions of impurities and dopants. Therefore, the powder standards were taken off from

Table 1. Investigated sintered ceramics. The raw materials are given as footnotes

Material	*Impurities, additives (wt%)*	*Grain sizes (sintered microstructure) (μm)*	*Grain boundary microstructure (Results of high resolution TEM studies)*
Al_2O_3*	0·001 Si, 0·001 Fe	0·4–2·5	Grain boundary facets free of amorphous phases, very few amorphous triple junctions
Al_2O_3 from boehmite†	0·16 Ti, 0·018 Si	0·5	Not investigated
Al_2O_3††	0·095 Si, 0·085 Mg, 0·065 Pb	2·5–9	Coexistence of interfaces with an amorphous phase and of facets free of any glass
ZrO_2(3 mol% Y_2O_3)‡	0·015 Na, 0·015 Fe, 0·010 Al	0·25–1	Continuous very thin amorphous interface in all grain facets (<1 nm)

*Taimicron DAR, Taimei Chemicals, Japan; 99.99% purity, specific surface (BET) 14 m^2/g, median particle size 0·2 μm.
†Disperal, Condea Chemie, Hamburg, Germany, specific surface (BET) 170 m^2/g, median particle size 5–10 nm.
††Alcoa A16SG, Aluminum Corp. of America, Bauxite, AR, 99.9% purity, specific surface (BET) 9 m^2/g, median particle size 0·6 μm.
‡TZ-3Y, Tosoh, Japan; 99.95% purity, specific surface (BET) 17 m^2/g, median particle size 60 nm.

the batches used to fabricate the sintered specimens *after* processing with all additives just before compaction and sintering, and they were annealed with the same temperature regime as applied to sinter the polycrystalline samples.

The X-ray measurements for alumina microstructures with grain sizes <3 μm and for all zirconia specimens were performed with Co–Kα radiation at 40 kV/40 mA; for coarser alumina microstructures (≥3 μm) Cu–Kα was used. The goniometers had a symmetric Bragg–Brentano arrangement (pw1820 with an analysing software APD1700* for alumina specimens with grain sizes <1 μm, HZG4† for all other samples). A secondary monochromator was used to improve the peak–background ratio. The software calculates the exact peak positions by a Marquardt non-linear least-squares fit. The algorithm continues the iterations until either a maximum number of 25 iterations has been performed or convergence has been reached. The default convergence criterion is ≤0·0001 or less fractional change per iteration in each of the twelve intrinsic parameters. After each iteration, the weighted sum of the squares indicates profile fitting's progress. The accuracy of the determined peak positions was ±0.005–0.010° due to a long measuring time of 20 s per step and a narrow step width $\Delta(2\Theta) = 0.02°$ which is less than 1/30 of the typical half-width of investigated reflexes.

The measuring range was $110° < 2\Theta < 145°$ with cobalt radiation. It contains sufficiently strong reflexes with different orientations of lattice planes with respect to the c-axis (Table 2). Due to the special preparation of the standards, only the residual stresses give rise to the measured difference in the X-ray peak positions

$$\Delta\Theta_{hkl} = \Theta_{hkl}^{specimen} - \Theta_{hkl}^{standard} \qquad (3(a))$$

and the related orientation dependent strain[26]

$$\varepsilon_{hkl} = -\Delta\Theta_{hkl}\cot\Theta_{hkl}\,, \qquad (3(b))$$

where Θ_{hkl} is the Bragg angle. The accuracy of the determined peak positions as stated above means errors of $0{\cdot}3 \times 10^{-4}$–$0{\cdot}5 \times 10^{-4}$ in the strain and of 10–20 MPa in the tension component of the residual microstress.

The use of eqn (3(b)) to derive an information about second kind residual microstresses requires that (i) the sample is free of macroscopic residual stresses or can be corrected for such effects, (ii) the microstresses are hydrostatic, (iii) surface effects resulting from small penetration depths and large grain sizes can be neglected. The first condition we shall discuss in Section 2.2. As to the other conditions, Fig. 2 demonstrates that the penetration depth

*Philips Ind. Electr. BV, Almelo, Netherlands.
†Richard Seifert & Co. Freiberger Präzisionsmechanik GmbH, Freiberg, Germany.

Table 2. Characterization of investigated reflexes (Al_2O_3: hexagonal indices for structural cell with c/a = 2·73). φ is the inclination of the lattice-plane normal to c-axis, Φ is the angular direction around the c-axis in Al_2O_3 as defined by Wachtman *et al.*[25] The Bragg angle Θ refers to Co–Kα radiation. The asterisk marks reflexes measured for coarser alumina microstructures (>3 μm) only

Material	*Reflexes*	*Orientation* φ	Φ	*Bragg reflection* 2Θ
Al_2O_3	(000·12)	0·0°	—	111·3
	(11$\bar{2}$·15)*	20·0°	0·0°	142·3
	(21$\bar{3}$·10)	40·0°	−10·5°	127·3
	(04$\bar{4}$·10)*	51·6°	−30·0°	145·2
	(22$\bar{4}$6)	61·2°	0·0°	118·1
	(41$\bar{5}$6)*	67·4°	−19·0°	136·1
	(13$\bar{4}$4)	71·0°	+16·0°	112·1
	(40$\bar{4}$4)	72·4°	−30·0°	131·2
	(04$\bar{4}$2)	81·0°	+30·0°	123·0
ZrO_2	(105)	16·0°	—	127·8
	(204)	36·0°	—	116·6
	(303)	55·0°	—	130·1
	(312)	66·0°	—	118·0
	(321)	79·0°	—	131·3

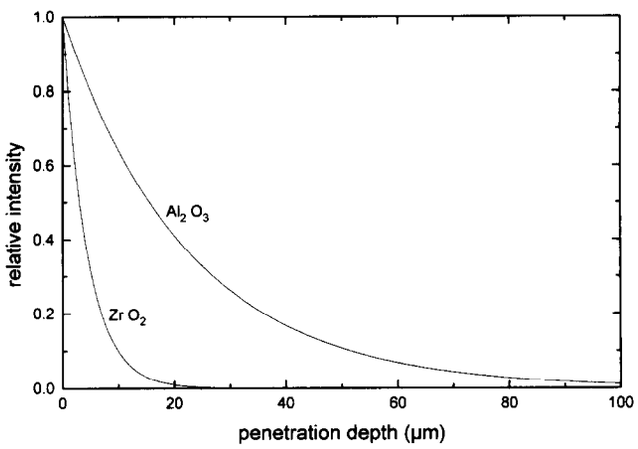

Fig. 2. X-ray intensity of Co–Kα radiation at $2\Theta = 120°$ as a function of the penetration depth in alumina and in zirconia.

of the X-rays is much larger than the grain sizes of the examined ceramics. Calculations show that the penetration depth (perpendicular to the surface) is almost independent of (hkl): the width of the range for the reflexes in Table 2 is 10·5% for Al_2O_3 and 6·5% for ZrO_2. Hence, most of the reflecting grains are in a depth below the surface that avoids surface effects.

2.2 Analysis of measured data

In Figs 3(a) and (b) the full curves exemplify the orientation dependence of the thermal anisotropy strains ε_{hkl} in Al_2O_3 and ZrO_2 calculated with an isotropic approximation by the same procedure as used for Fig. 1 (orientation averages of the elastic parameters E and ν as given in the introduction. As an example, strain states are selected which finally would give a corresponding maximum tension in c-axis direction of $\sigma_{33} = +100$ MPa in both materials.

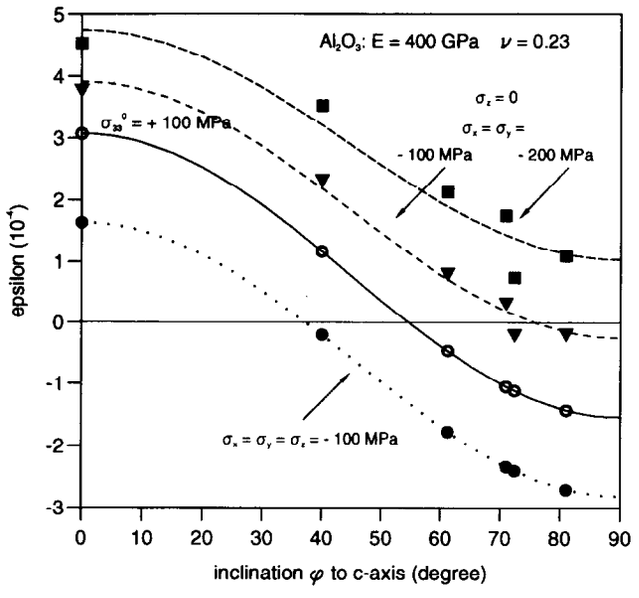

(a)

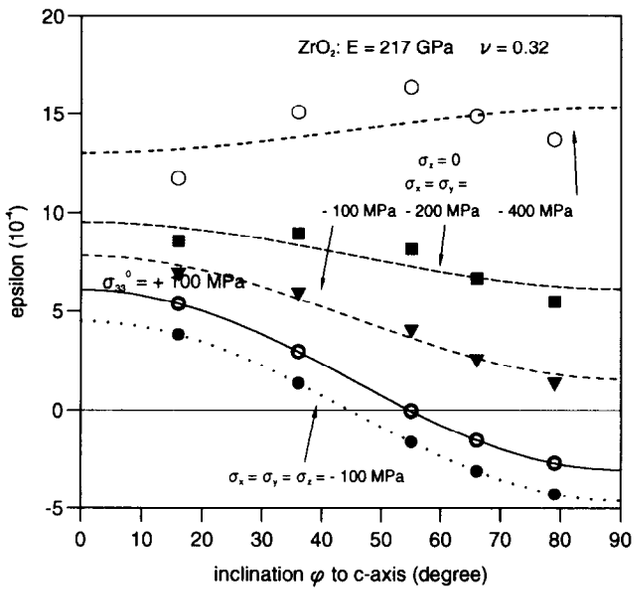

(b)

Fig. 3. Influence of elastic anisotropy and of superpositioned first kind residual surface stresses in Al_2O_3 (Fig. 3(a)) and in ZrO_2 (Fig. 3(b)) on deviations of TEA strain ε_{hkl} from an isotropic (cosine-like) approximation. Full symbols give results for selected reflexes calculated by eqns (5) and (6). Full lines—pure TEA stresses; broken lines—effect of superpositioned plain surface compression; dotted lines—superposition with hydrostatic compression.

With the exception of the broken sol/gel derived reference sample, all X-ray investigations were performed on ground surfaces where first kind residual stresses should be present. In comparison with the macrostress-free material (full curves in Fig. 3), the probable compressive character of these plane macrostresses (component normal to the surface $\sigma_z = 0$) produces an additional *positive* strain perpendicular to the surface because all reflecting lattice planes are oriented here with their normals parallel to the surface normal (Fig. 3 also demonstrates that *hydrostatic* compression would be required to reduce the TEA strain). Of course, these macrostresses would violate the condition (i) given above for the application of eqn (3(b)), and an appropriate correction is required.

It has been shown that under the assumption of elastic isotropy macrostresses simply shift the orientation dependent strain curves which characterize the pure type II microstresses in Fig. 3; the amount of this shift equals the level of the superpositioned macrostress.[27] This behaviour provides a way to calculate both the TEA microstress and the macrostress by re-shifting the measured strain curves to a zero position at an inclination angle = 54·7° or, in other words, to a position where $\varepsilon_{33} = -2\ \varepsilon_{11}$ (the characteristics of the macrostress-free state in Fig. 3). Unfortunately, the situation becomes more complicated if elastic anisotropy causes systematic deviations from the cosine-like curve derived under the assumption of elastic isotropy and alters the character of the curve-shift produced by macrostresses. In Al_2O_3, these effects are probably small: no systematic and significant deviation was observed for 6 investigated reflexes in 7 specimens. Investigations of 5 reflexes in 7 ZrO_2 samples sometimes showed (105) data below and (321) strains above the cosine-like fit, but generally the deviations were of random character either in ZrO_2. It was, nevertheless, decided to separate the actually interesting TEA stresses and possible macrostresses with consideration of elastic anisotropy. The reason was to be sure that deviations of the measured ε_{hkl} (φ) curve from the form expected for pure type II TEA-stresses are really associated with the superposition of macrostresses and not generated by elastic anisotropy alone.

Grigoryev described a way to take into consideration the elastic anisotropy for the analysis of these first kind surface stresses.[28] Generally, the strain component perpendicular to the specimen surface in the laboratory-coordinate system of the measurement (where the z-axis is perpendicular to the surface) is calculated with the compliances s_{33ij} according to

$$\varepsilon_{33} = \sum_{j=1}^{3} (s_{331j}\,\sigma_{1j} + s_{332j}\,\sigma_{2j} + s_{333j}\,\sigma_{3j})\,. \qquad (4)$$

The tensor components s_{33ij} and the stresses σ_{ij} have to be derived from the data in the crystallographic-coordinate system by corresponding transformations. Grigoryev gives solutions for the cubic system[21,28] which are used here as a sufficient approximation for ZrO_2 (3 mol% Y_2O_3) with its very small tetragonality. Tensorial calculations for the trigonal system were performed for Al_2O_3. Since hydrostatic stress fields

cannot exist in single phase polycrystals by physical reasons, only results for plane surface compression $\sigma_{SF} = \sigma_x = \sigma_y$ ($\sigma_z = 0$) are given here. With the orientation angles φ (inclination of the lattice-plane normal to c-axis) and Φ (the angular direction around the c-axis) as defined by Wachtman *et al.*[25] the resulting equations are:

Al_2O_3

$$\varepsilon_{33}/\sigma_{SF} = (s_{11} + s_{33} - s_{44})\sin^2\varphi\cos^2\varphi + s_{12}\sin^2\varphi + s_{13}(\sin^2\varphi + 2\cos^4\varphi) + 2s_{14}\sin^3\varphi\cos\varphi\sin\Phi(1 - 4\cos^2\Phi) \quad (5)$$

For the quantitative evaluation, the s_{mn} matrix components published by Wachtman *et al.*[25] were used here.

ZrO_2

$$\varepsilon_{33}/\sigma_{SF} = 2s_{12} + 2(s_{11} - s_{12} - 0{\cdot}5s_{44})\Gamma \quad (6)$$

orientation factor $\Gamma = (h^2k^2 + k^2l^2 + h^2l^2)/(h^2 + k^2 + l^2)$

The elastic compliances were derived for ZrO_2 (3 mol% Y_2O_3) from data published by Ingel *et al.*[29]: $s_{11} = 2{\cdot}735 \times 10^{-3}$ GPa^{-1}, $s_{12} = -5{\cdot}763 \times 10^{-4}$ GPa^{-1}, $s_{44} = 1{\cdot}842 \times 10^{-2}$ GPa^{-1}.

The individual points in Fig. 3 represent these calculations for some of the reflexes (Table 2); the broken and dotted lines are results of a least squares fit. Contrary to hydrostatic first kind residual stresses, with a plane surface stress ($\sigma_z = 0$) elastic anisotropy causes considerable deviations from the (isotropic approximation) TEA fit, and in zirconia the whole character of the ε_{hkl} (φ) dependence can change.

The analysis of the measured ε_{hkl} data was performed as illustrated in Fig. 4 for the example of an alumina microstructure with a grain size of 1·9 μm:

(1) The measured Θ_{hkl} of sintered specimen and powder standard give ε_{hkl} by eqn (3).

(2) The measured ε_{hkl} (φ) are influenced by superpositioned first kind surface stress as demonstrated by Fig. 3: compared with the macrostress-free curve, a result of higher measured ε_{hkl} (φ) requires a correction for plane compression σ_{SF} (lower ε_{hkl} (φ) would indicate hydrostatic compression σ_{HY}). A cosine-like least squares fit of measured (1) and corrected (2) ε_{hkl} was achieved with a stepwise variation of the macrostresses σ_{SF} by a computer program that finally stopped at $\varepsilon_{33} = \varepsilon_{fit}$ ($\varphi = 0°$) $= -2\,\varepsilon_{11} = -2\varepsilon_{fit}$ ($\varphi = 90°$). The use of a cosine-like function minimizes the fitting error in the final result ε_{33}. Note that the significance of this ε_{33} is high because it represents the full information of *all* measured ε_{hkl}. The relevant equations for Al_2O_3 and ZrO_2 are (5) or (6) for plane surface compression $\sigma_{SF} = \sigma_x = \sigma_y$ ($\sigma_z = 0$), the macrostress levels are given by the end point of the variation procedure.

Most of the specimens exhibited measured ε_{hkl} as in the example of Fig. 4 and enabled a ready analysis assuming plane surface compression (σ_{SF} is –50... –100 MPa for the coarsest and –100...–200 MPa for the fine grained alumina microstructures; similar values are observed for most ZrO_2 samples with one exception of –370 MPa in the 0·3 μm microstructure).

However, a measurement of two submicron alumina specimens with extremely low resulting microstresses of 20–30 MPa (i.e. close to the limit given by the measuring accuracy of 10–20 MPa) showed all negative ε_{hkl} the interpretation of which would require the assumption of a small *hydrostatic* compression or of a plane *tension* stress in the surface. Both explanations must be discarded, the first by physical reasons and the second due to the known compressive character of macrostresses in ground ceramics. More probably, such (small) apparently negative ε_{hkl} are associated with occasional slight stresses in the annealed powder standards: sintering of submicron samples requires raw materials with grain sizes of 150 nm and less, and due to this fine grain size the annealing procedure of the powder standards may well happen to cause some slight degree of sintering even in the loose powder. The consequence is an additional error in $\Theta_{hkl}^{standard}$ in eqn (3(a)) which is insignificant when $\Delta\Theta_{hkl}$ is large but may become important if this difference is close to zero. The contribution to the possible error in σ_{33} is about 5 MPa.

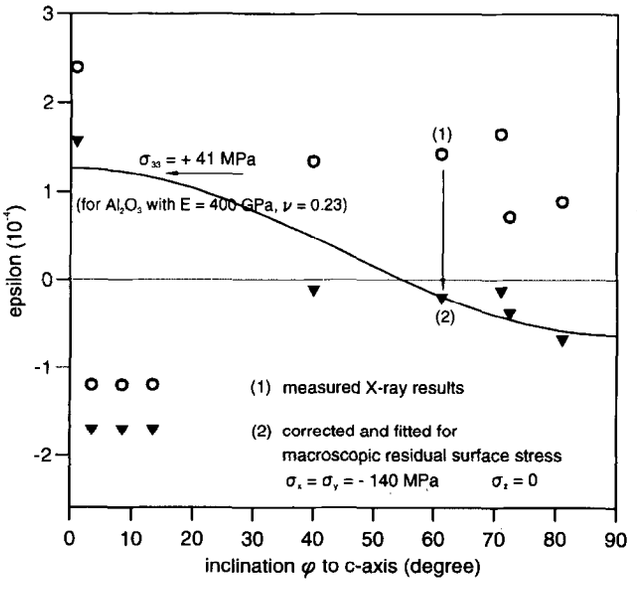

Fig. 4. Illustration of the subsequent steps of the analysis (example: measured strain data ε_{hkl} in a 1·9 μm alumina microstructure). Step (2) also considers elastic anisotropy (eqns (5) and (6)).

The final ε_{33} resulting from the variation procedure gives the average TEA tensile stress component for c-axis orientation with the elastic isotropic approach discussed in the introduction by

$$\sigma_{33} = \frac{E_{\text{eff}}}{(1 + \nu_{\text{eff}})} \varepsilon_{33} \qquad (7)$$

with the given orientation averages for E_{eff} and ν_{eff}. The total amount of all contributions to a possible maximum error is about ±25 MPa in σ_{33}.

3 Results

Figure 5 displays the grain size influence on the TEA residual stress measured for alumina microstructures with grain sizes between 0·3 and 9 μm. Here as in the following figure the tensile component in the c-axis direction resulting from the cosine-like fit of all measured ε_{hkl} is used as a representative parameter that contains all information about the whole orientation dependence of TEA stresses in a microstructure. Note that this double-logarithmic plot must not be used for extrapolations into the range of coarser grain sizes because it neglects the existence of an upper (relaxation-free) stress limit (calculated in Fig. 1).

In Fig. 5, the data point at a grain size of 0·5 μm represents the sol/gel derived broken reference sample. This microstress is in no way distinguished from the results obtained on ground surfaces and gives convincing evidence for the sound basis of the procedure adopted here to separate type I and type II residual stresses in the analysis.

Figure 6 compares TEA residual stresses for ZrO_2 and Al_2O_3 in analogy with Fig 5. The measured TEA stresses are similar in Al_2O_3 and in ZrO_2 for

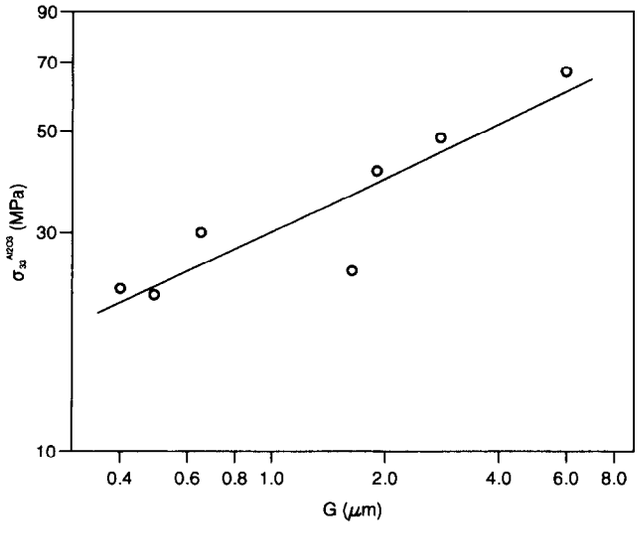

Fig. 5 Double-logarithmic presentation of the grain size influence on TEA residual stress in alumina.

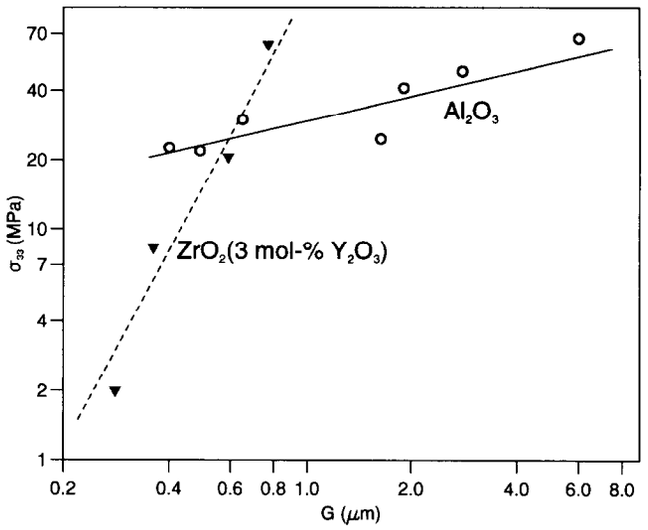

Fig. 6. Comparison of TEA residual stresses in submicron zirconia and alumina.

grain sizes in the range 0·5 – 1 μm, but considering the results of the finer grained microstructures, Fig. 6 suggests different grain size effects. However, the error of ±25 MPa as discussed above indicates a limited reliability of all stress results <30 MPa. Since most of the zirconia data are within or close to this range, no final conclusion about the grain size effect in tetragonal zirconia should be derived here. As a consequence, it is also impossible to advance reliable suggestions about the residual stresses in coarser zirconia ceramics, and the experimental comparison with alumina in analogy with the calculated data in Fig. 1 remains an open issue.

4 Discussion

Due to relaxation, the thermal expansion anisotropy stresses σ_{33} in alumina given in Fig. 5 are lower than the relaxation-free solution in Fig. 1. Figure 5 corresponds well with the result of +56 MPa obtained by optical fluorescence[23] for 2–8 μm grain size alumina in Al_2O_3/ZrO_2 composites, but there is poorer agreement with the published 100–160 MPa reported for single phase alumina of the same grain size.[24] Two comments are possible. On the one hand, the consistency of our results for the whole grain size range 0·3 μm < G < 9 μm in Fig. 5 indicates a fairly high degree of significance of the present results on a qualitative level. On the other hand, the limits of accuracy indicate that also the present results do not exclude a TEA tensional component σ_{33} close to + 100 MPa with grain sizes of about 10 μm, and present and previous results will come close to each other. This idea becomes further substantiated if we remember that just the coarser

alumina specimens in the present investigations contain dopants and impurities which favour relaxation.[22] Hence, slightly higher TEA stresses than the upper limit observed in the present investigations are probable with an improved purity at grain sizes of about 10 μm.

Contrary to the comparison with previously published experimental data, it is difficult to compare the present results for alumina with a *theoretically* predicted grain size effect. As outlined in the introduction, the existing models do not provide a ready functional dependence of residual stresses on the grain size, and approximations that give an inverse grain size effect $1/G^3$ are ruled out by our results. Replotting the data of Fig. 5 as a function of $1/G^3$ gives a linear relationship but with σ_0 = 60–70 MPa which is an unlikely result compared with the calculated relaxation-free stress level of 150 MPa suggested by Fig. 1.

The double-logarithmic plot of all alumina σ_{33} data between 0·3 and 9 μm in Fig. 5 indicates *one* grain size dependent relaxation mechanism of the TEA microstresses σ_{TEA} in fine and in medium grained alumina according to $\sigma_{TEA} \sim G^m$ with m $\approx$ 0·39. This value is close to m $\approx$ 0·37 which may be derived by a logarithmic plot of the data obtained by Ma and Clarke[24] for alumina microstructures with grain sizes ranging from 2 to 16 μm. If we compare with the much smaller grain size effect calculated by Blendell and Coble[17] (6 MPa difference for grain sizes between 50 and 150 MPa) we have to consider that the influence of the grain size must decrease when approaching the relaxation-free conditions at very large grain sizes.

A similar decrease of the grain size influence occurs at extremely fine grain sizes. A closer inspection of Fig. 5 considering the logarithmic character reveals a behaviour which actually is similar to a lower limit of the relaxation. To reduce the grain sizes from about 5–10 μm to approximately 1–2 μm causes a drop of the residual stress component σ_{33} by about 50% (about –35 MPa). In the investigated submicrometer range, however, the absolute changes in σ_{33} become very small. This behaviour compares well with general expectations and is, of course, consistent with the theoretical models as discussed in the introduction.

The TEA residual stresses of the 0·5 μm sol/gel-derived alumina microstructure are consistent with all other data in Fig. 5. Obviously, the TEA microstresses as obtained here are independent of special technological approaches and surface conditions.

The evaluation of the results at very small grain sizes and low microstresses is considerably influenced by the accuracy of the measurements. The extremely thin amorphous grain boundary interface in ZrO_2 (0·5 nm) that is know to promote superplastic deformation (at very *slow* rates) and may cause a stronger grain size effect with extremely small residual microstresses in tetragonal zirconia at grain sizes <0·5 μm. However, at present no sufficiently precise measuring approach is available to draw valid conclusions about microstress components <15 MPa in single phase ceramics. Most of the investigated zirconia microstructures exhibit results close to or lower than the accuracy of the measurement. With the present data it is, therefore, impossible to draw final conclusions about the relaxation behaviour of microstresses in zirconia. Experiments with coarser microstructures would be required to compare the relaxation-free state of zirconia with the calculated result in Fig. 1, but the known phase instability of tetragonal zirconia at larger grain sizes will make such investigations very difficult if not impossible.

5 Conclusions

In sintered alumina, the average tensional component in x-axis direction is about 30–100 MPa with grain sizes of 1–9 μm. With smaller grain sizes 0·3–1 μm, this stress component is reduced further due to known relaxation processes, but the absolute changes are small in the submicrometer range: the investigations suggest a level of about 20–30 MPa. However, at present no sufficiently precise measuring approach is available to draw valid conclusions about microstress components <30 MPa in single phase ceramics.

A double-logarithmic plot gives a consistent grain size dependence close to $\sigma_{TEA} \sim G^{1/3}$ for the whole range of investigated grain sizes 0·3 μm < G < 9 μm. It is, therefore, suggested that there is no change in the fundamental relaxation processes within the investigated range of grain sizes. At present, there is no basis for a ready comparison of the observed grain size influence with existing theoretical models.

With grain sizes between about 0·5 and 1 μm, the residual stresses measured in tetragonal zirconia polycrystals are similar as observed in alumina (20–60 MPa). However, the stresses in microstructures with grain sizes 0·2–0·4 μm are actually smaller than the limit of accuracy (probably <10 MPa). Therefore, no final conclusions can be derived here for the grain size effects in this material.

The comparison of residual TEA stresses in compact, ground alumina samples produced by a powder technological approach and in equally dense grit samples of sol/gel origin reveals that the present results are independent of special processing routes and surfaces states.

Acknowledgments

The investigations at the Dresden Fraunhofer Institute have been supported in part by the Deutsche Forschungsgemeinschaft under contract Kr 1398/1-1. We gratefully acknowledge the cooperation with Dr W. Kreher at the Max-Planck-Group of the Mechanics of Heterogeneous Solids in Dresden (Germany) and with Dr E. Pippel and Dr J. Woltersdorf at the Max-Planck-Institute of Microstructural Physics in Halle (Germany).

References

1. Kloos, K. H., Eigenspannungen, Definition und Entstehungsursachen (Residual stresses, definition and origin). *Z. Werkstofftechnik*, **10**(9) (1979) 293–302.
2. Hockey, B. J., Observations by transmission electron microscopy on the subsurface damage produced in aluminium oxide by mechanical polishing and grinding. *Proc. Brit. Ceram. Soc.*, **20** (1972) 95–115.
3. Hockey, B. J., Plastic deformation of aluminum oxide by indentation and abrasion. *J. Am. Ceram. Soc.*, **54**(5) (1971) 223–31.
4. Xu, H. & Jahanmir, S., Effect of microstructure on subsurface damage and material removal in grinding of alumina ceramics. Paper SXI-35-94 in *96th Annual Meeting Abstracts*, The America Ceramic Society, Westerville, Ohio, 1994.
5. Samuel, R., Chandrasekar, S., Farris, T. N. & Licht, R. H., Effect of residual stresses on the fracture of ground ceramics. *J. Am. Ceram. Soc.*, **72**(10) (1989) 1960–6.
6. Scholtes, B., Recent investigations on the origin and distributions of residual stresses in ceramics and metal-ceramic compounds. In *Constraints Résiduelles et Nouvelles Téchnologies*, CETIM, Paris, 1990, pp. 61–71.
7. Evans, A.G., Microfracture from thermal expansion anisotropy—I. Single phase systems. *Acta Metall.*, **26**(12) (1978) 1845–53.
8. Wu, C. Cm., Freiman, S. W., Rice, R. W. & Mecholsky, J. J., Microstructural aspects of crack propagation in ceramics. *J. Mater. Sci.*, **13**(12) (1978) 2659–70.
9. Green, D. J., Microcracking mechanisms in ceramics. In *Fracture Mechanics of Ceramics*, Vol. 5, ed. R. C. Bradt, A. G. Evans, D. P. H. Hasselman & F. F. Lange. Plenum Press, New York, 1983, pp. 457–78.
10. Heuer, A. H. & Rühle, M., On the nucleation of the martensitic transformation in zirconia (ZrO_2). *Acta Metall.*, **33**(12) (1985) 2101–12.
11. Schmauder, S. & Schubert, H., Significance of internal stresses for the martensitic transformation in yttria-stabilized tetragonal zirconia polycrystals during degradation. *J. Am. Ceram. Soc.*, **69**(7) (1986) 534–40.
12. Becher, P. F. & Ferber, M. K., Grain-size dependence of the slow-crack growth behaviour in noncubic ceramics. *Acta Metall.*, **33**(7) (1985) 1217–21.
13. Fu, Y. & Evans, A. G., Microcrack zone formation in single-phase polycrystals. *Acta Metall.*, **30**(8) (1982) 1619–25.
14. Pompe, W. & Kreher, W., Theoretical approach to energy-dissipative mechanisms in zirconia and other ceramics. In *Advances in Ceramics, Vol. 12 (Zirconia 11)*, ed. N. Claussen, M. Rühle & A. H. Heuer. The American Ceramic Society, Columbus, Ohio, 1983, pp. 283–92.
15. Kreher, W., Residual stresses and stored elastic energy of composites and polycrystals. *J. Mech. Phys. Solids*, **38**(1) (1990) 115–28.
16. Kreher, W. & Molinari, A., Residual stresses in polycrystals as influenced by grain shape and texture. *J. Mech. Phys. Solids*, **41**(12) (1993) 1955–77.
17. Blendell, J. E. & Coble, R. L., Measurement of stress due to thermal expansion anisotropy in Al_2O_3. *J. Am. Ceram. Soc.*, **65**(3) (1982) 174–8.
18. Evans, A. G. & Clarke, D. R., Residual stresses and microcracking induced by thermal contraction inhomogeneity. In *Thermal Stresses in Materials and Structures*, ed. D. P. H. Hasselman & R. A. Heller. Plenum Press, New York, 1980, pp. 629–48.
19. Green, D. J., Lange, F. F. & James, M. R., Factors influencing residual surface stresses due to a stress-induced phase transformation. *J. Am. Ceram. Soc.*, **66**(9) (1983) 623–9.
20. Eigenmann, B., Scholtes, B. & Macherauch, E., Determination of residual stresses in ceramics and ceramic–metal composites by X-ray diffraction methods. *Mater. Sci. Eng. A*, **118**(5) (1989) 1–17.
21. Grigoryev, O. N. & Krivoshei, G. S., Determination of thermal stresses in heterogeneous materials (in Russian). *Zavodskaya Laboratoria*, 7/8 (1992) 30–2.
22. Krell, A. & Grigoryev, O. N., Residual stresses and microporosity in oxide ceramics. *Sprechsaal*, **123**(10) (1990) 1012–15.
23. Ma, Q., Pompe, W., French, J. D. & Clarke, D. R., Residual stresses in Al_2O_3–ZrO_2 composites: A test of stochastic stress models. *Acta Metall. et Mater.*, **42**(5) (1994) 1673–81.
24. Ma, Q. & Clarke, D. R., Piezospectroscopic determination of residual stresses in polycrystalline alumina. *J. Am. Ceram. Soc.*, **77**(2) (1994) 298–302.
25. Wachtman Jr., J. B., Tefft, W. E., Lam Jr., D. G. & Stinchfield, R. P., Elastic constants of synthetic single crystal corundum at room temperature. *J. Res. Nat. Bureau of Standards - A.*, **64**(3) (1960) 213–28.
26. Grigoryev, O. N., Krell, A., & Trefilov, V. I., Determination of thermal residual stresses in single-phase ceramic materials (in Russian). *Zavodskaya Laboratoria*, 7 (1990) 36–9.
27. Kreher, W., Pompe, W., *Internal Stresses in Heterogeneous Solids*. Akademie-Verlag, Berlin, 1989.
28. Grigoryev, O.N., Thesis submitted for the degree of a Doctor of Sciences (habilitation). Ukrainian Academy of Sciences, Kiev, 1992.
29. Ingel, R. P., Lewis III, D., Elastic anisotropy in zirconia single crystals. *J. Am. Ceram. Soc.*, **71**(4) (1988) 265–71.